THE JOURNAL OF PHYSICAL CHEMISTRY B

Article

pubs.acs.org/JPCB

Electrophoretic Deposition of TiO_2/Er^{3+} Nanoparticulate Sols

Mario Borlaf,[†] María Teresa Colomer,[†] Fátima Cabello,[‡] Rosalia Serna,[‡] and Rodrigo Moreno*,[†]

[†]Instituto de Cerámica y Vidrio, CSIC, C/Kelsen, 5, E-28049, Madrid, Spain

[‡]Instituto de Óptica "Daza de Valdés", CSIC, C/Serrano, 121, E-28006, Madrid, Spain

ABSTRACT: TiO_2 and TiO_2/Er^{3+} nanoparticulate sols were obtained by the colloidal sol−gel route. Thanks to the combination of three optical techniques (laser diffraction, LD, dynamic light scattering, DLS, and multiple light scattering, MLS), the peptization time was quantified, demonstrating that erbium(III) ions retard the process. The isoelectric point of TiO_2 shifts up to higher pH's when Er^{3+} ions are present, which suggests that they are adsorbed onto the surface of the TiO_2 nanoparticles. Moreover, the viscosity of the sols increases when the erbium(III) amount increases. The xerogels obtained from each sol were characterized by XRD and HRTEM, obtaining in all cases anatase as the major phase, although traces of brookite were also present. In the EPD experiments, the addition of ethanol was necessary to reduce the water hydrolysis and facilitate the drying process. As a result, transparent thin films were obtained at short times and low current densities and opal films for larger current densities and deposition times; in addition, the thickness, measured by ellipsometry, increased gradually, but the refractive index did not change significantly (1.9−2). The topography profile of the films and the particle size were obtained by atomic force microscopy (AFM), giving similar values to those measured by DLS, indicating that the addition of ethanol helps to maintain stabilization without further agglomeration or sedimentation.

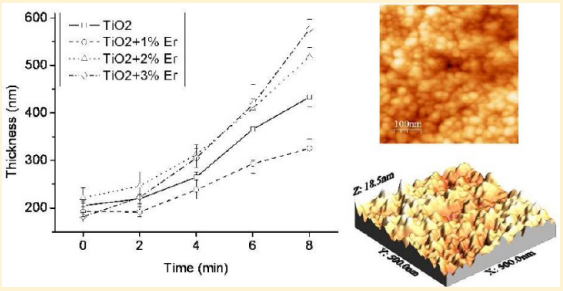

INTRODUCTION

Electrophoretic deposition (EPD) is a powerful technique for the production of thin and thick coatings on conductive substrates. EPD is a processing technique with high versatility both in the product specifications and in the experimental setup used for the deposition, which can be done under different conditions and numerous modifications such as continuous[1] or pulsed[2] voltage or intensity, and different shapes of the electrodes depending on the product to be obtained (coatings of wires, tube walls, infiltration of porous materials, etc.)[3,4] or applying a magnetic field to obtain crystalline-oriented structures,[5] among others. In all cases, the use of one or another depends always on the need to obtain thin[6] or thick[7] films for different applications such as fuel cells,[1] micro-batteries,[5] solar cells,[8] biomaterials,[9] traditional ceramics,[10] etc. Thin films are usually obtained using specific deposition techniques as spin-coating or dipping, but thicker films and higher reproducibility can be obtained by EPD using well-dispersed suspensions. In spin coating, the lower reproducibility is due to the expulsion of the suspension when the substrate starts to rotate; in dipping, there is a border effect at the bottom of the coated substrate that swells down by gravity, especially when suspensions are prepared in a nonvolatile solvent like water. Both techniques have the same problem of lack of homogeneity, which is more pronounced when the particle size and the film thickness decrease.

One of the most promising applications of EPD to produce thin films is in the field of catalysis. In particular, TiO_2 is a material which is being used for this goal under UV light,[11] but it has also great interest for different applications such as gas sensor,[12] hydrogen storage,[13] etc.[10] Furthermore, the limited properties of TiO_2 can be improved or strongly changed with the addition of dopants. This is the case of rare earth (RE) elements which contribute with photoluminescent properties. One application of this kind of materials is as wave guides.[14] In the case of erbium(III), the main transition is between the first excited state and the ground state ($^4I_{13/2} \rightarrow {}^4I_{15/2}$) and depends on different parameters such as the oxidation state, its location in the lattice, and the crystallization state around the dopant.[14]

Different synthesis routes have been developed to obtain TiO_2/Er^{3+} materials, i.e., polymeric sol−gel,[14] ion-implantation,[14] hydrothermal synthesis,[15] etc., and different deposition techniques such as dipping[14] or laser ablation[16] were used for the preparation of the thin films. In this work, an easy synthesis has been performed using the colloidal sol−gel method to obtain stable and monomodal nanoparticulate sols; moreover, the thin films were prepared by EPD on 316 L stainless steel substrates in galvanostatic conditions. Peptization time, particle size evolution, zeta potential, viscosity, and optical properties of the sols were studied, XRD and HRTEM-EDX were used to characterize the xerogels, and the ellipsometry technique was employed to measure the thickness and the refractive index of the thin films.

Special Issue: Electrophoretic Deposition

Received: April 26, 2012
Revised: July 13, 2012
Published: July 16, 2012

dx.doi.org/10.1021/jp304044w | J. Phys. Chem. B 2013, 117, 1556−1562

EXPERIMENTAL SECTION

Sol Preparation and Characterization. The alkoxide hydrolysis was carried out by adding titanium(IV) isopropoxide (97%, Sigma-Aldrich, Steinheim, Germany) to a stirring mixture of deionized water (18.2 MΩ·cm^{-1}, ultrapure Milli-Q) and nitric acid (Merck, Darmstadt, Germany) in a water:alkoxide molar ratio of 50:1. In TiO_2/Er^{3+} sols, before the addition of the alkoxide, erbium(III) acetate hydrate ($Er(OOCCH_3)_3{\cdot}xH_2O$, Sigma-Aldrich, Steinheim, Germany) was dissolved in the mixture of water and nitric acid to a molar ratio Er^{3+}/TiO_2 of 1, 2, and 3%. The synthesis temperature was maintained constant during the entire process at 35 °C. HNO_3 (65%, PANREAC, Barcelona, Spain) was used as a catalyst in a molar ratio of H^+/Ti^{4+} = 0.2 in both cases.

The evolution of the average particle size ($D_{v,0.5}$) was studied as a function of the synthesis time. The particle sizes of the agglomerates and/or aggregates were measured by laser diffraction (LD, Mastersizer, Malvern S, Worcestershire, U.K.) until the diameter was beyond the detection limit of the instrument. For smaller sizes, dynamic light scattering (DLS, Zetasizer Nano ZS, Malvern S, Worcestershire, U.K.) was used until the end of the peptization process. At the same time, the measurements of the stability of the system were performed by multiple light scattering in the near-infrared (MLS-NIR, Turbiscan Classic MA 2000, Formulaction, Toulouse, France).

The zeta potential of the nanoparticulate sols (once the peptization was completed) was determined by laser doppler velocimetry with the same equipment as particle size, and measurements were performed with a concentration of the sols of 10^{-2} M in 10^{-2} M KCl. The variation of zeta potential as a function of pH was studied using 1 M KOH as a base. Finally, the viscosity of the sols was measured with a rotational rheometer (RS50, Haake, Thermo, Karlsruhe, Germany) with a double-cone/plate sensor configuration (DC60/2°, Haake, Thermo). The controlled rate (CR) program of this study was formed by three stages: a linear increase of the shear rate from 0 to 1000 s^{-1} in 300 s, a plateau at 1000 s^{-1} for 60 s, and a decrease to zero shear rate in 300 s.

Xerogel Characterization. The xerogels of the respective sols were obtained drying at room humidity and temperature. The crystalline phases were identified by X-ray diffraction (XRD) (X'Pert PRO theta/2theta Panalytical, Almelo, Netherlands) and using the Scherrer equation[17] the crystal size (D_{XRD}) was calculated:

$$D_{XRD} = \frac{K\lambda}{\beta \cos\theta} \quad (1)$$

where K is the shape factor (0.9), λ is the X-ray wavelength (Cu Kα_1 = 1.54060 Å), β is the full width at half-maximum intensity (fwhm) in radians, and θ is the Bragg angle in degrees. The microstructure of the crushed xerogels was studied using high resolution transmission electron microscopy (HRTEM-EDX) working at 400 keV (JEOL JEM 4000EX, Tokyo, Japan).

EPD Tests and Thin Film Characterization. The sols were diluted in ethanol absolute (99.5%, PANREAC, Barcelona, Spain), until ~55 wt %, for the EPD experiments, which were performed in galvanostatic mode for current densities of ~0.25−1 mA·cm^{-2} (every 0.25 mA·cm^{-2}) and deposition times of 2−15 min (every 2 min), using a power source (KEITHLEY, mod. 2611, Ohio, USA). Steel foils (AISI 316 L, 2 × 4 cm^2) were used as electrodes, which were maintained at a separation distance of 1 cm. The coated substrates were extracted immediately after EPD (i.e., when the electric field is not applied) at a constant withdrawal rate of 0.5 mm·s^{-1} (that is, 3 cm·min^{-1}), and the films were dried at room temperature and humidity conditions. A general view of the thin films was obtained using an optical microscope (WITec/ALPHA 300 AR, WITec Wissenschaftliche Instrumente and Technologie GmbH, Ulm, Germany). The thickness and refractive index of the films were determined from variable angle ellipsometry analysis using a J.A. Woollam VASE ellipsometer (Lincoln, USA). The ellipsometric parameters were measured in the wavelength range from 300 to 1500 nm (every 10 nm) at angles of incidence of 60 and 70°. The analysis was performed assuming a two-layer system with flat and parallel interfaces composed by the steel substrate, considered as a semi-infinite medium, and the TiO_2 layer.[18] The refractive index of the TiO_2 layer was fitted by a Cauchy function. Finally, the topography images were obtained by an atomic force microscope (Nanotec Electronica, Madrid, Spain).[19]

RESULTS AND DISCUSSION

Sol Characterization. When the alkoxide is added to the acid solution, the hydrolysis and polycondensation reactions occur immediately due to the large amount of water with respect to the alkoxide. After that point, the peptization step starts thanks to the adsorption of the protons onto the surface of the TiO_2 agglomerates/aggregates which provokes the breaking of the agglomerates/aggregates by electrostatic forces giving nanoparticles in the media.[20]

There are two characteristic times defining the peptization of the nanoparticulate sols, corresponding to the time at which the agglomerates/aggregates start to break down into nanoparticles leading to a translucent sol (t_1) and the time at which the

Table 1. Peptization Times and Particle Sizes ($D_{v,0.5}$) of the Sols and Crystal Sizes of the Xerogels Calculated by Scherrer's Equation (D_{XRD}) and Observed by TEM (D_{TEM})

	$Dv,0.5$ (nm)	D_{XRD} (nm)	D_{TEM} (nm)	t_1 (h)	t_2 (h)
TiO_2	22	4.6		25	32
TiO_2+1%Er^{3+}	32	3.9		32	40
TiO_2+2%Er^{3+}	21	3.9	3.5	41	51
TiO_2+3%Er^{3+}	18	3.8		60	79

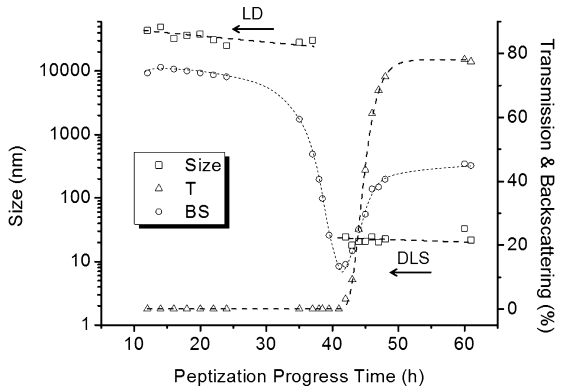

Figure 1. Laser difraction, LD, (□) dynamic light scattering, DLS, (□), and near-infrared transmitted light (backscattering ○, transmission △) measurements as a function of the peptization progress time for the TiO_2/Er^{3+} (2 mol %) sol.

dx.doi.org/10.1021/jp304044w | J. Phys. Chem. B 2013, 117, 1556−1562

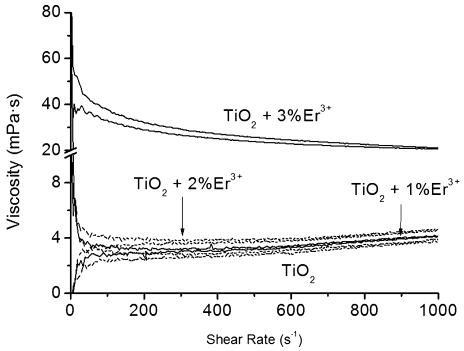

Figure 2. Viscosity curves of the peptized TiO_2 and TiO_2/Er^{3+} sols.

particle size and the optical properties (T, BS, and particle size) maintain constant with time (t_2) so that peptization has finished. It is possible to observe that particle size does not change significantly with the erbium(III) concentration, whereas the peptization time clearly increases. Table 1 shows the values of the different parameters at those characteristic times of peptization.

Figure 1 shows the evolution of the particle size and the transmission and backscattering of light registered during MLS measurements for nanoparticulate sols of TiO_2+2 mol % of Er^{3+} with time, according to the protocol established by Colomer et al.[20,21] Initially, the particle size was measured by LD because the sol hydrolyses and polycondensates immediately forming large agglomerates that are in the range of micrometers. This is the reason why the system shows a high value of backscattering (BS) and there is not transmission (T) of the light (the sample is opaque). Moreover, the MLS measurements show a sedimentation process because at the bottom of the cell the BS increases while at the top it decreases. Following the BS curve, a minimum value is found at ~41 h where some agglomerates and nanoparticles are observed by LD and DLS.

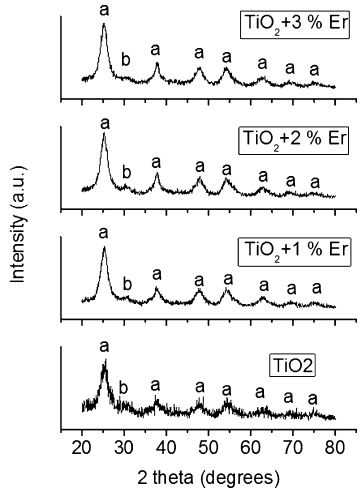

Figure 4. XRD patterns of the TiO_2 and TiO_2/Er^{3+} green xerogels. The anatase phase is labeled a and the brookite phase b.

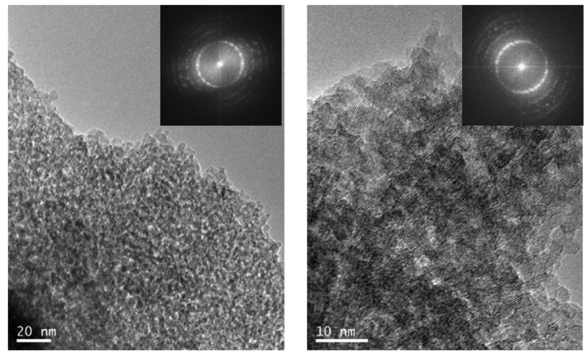

Figure 5. Transmission electron micrographs of the as-prepared TiO_2/Er^{3+} (2 mol %) xerogels. Fast Fourier transformation diagrams are shown as insets.

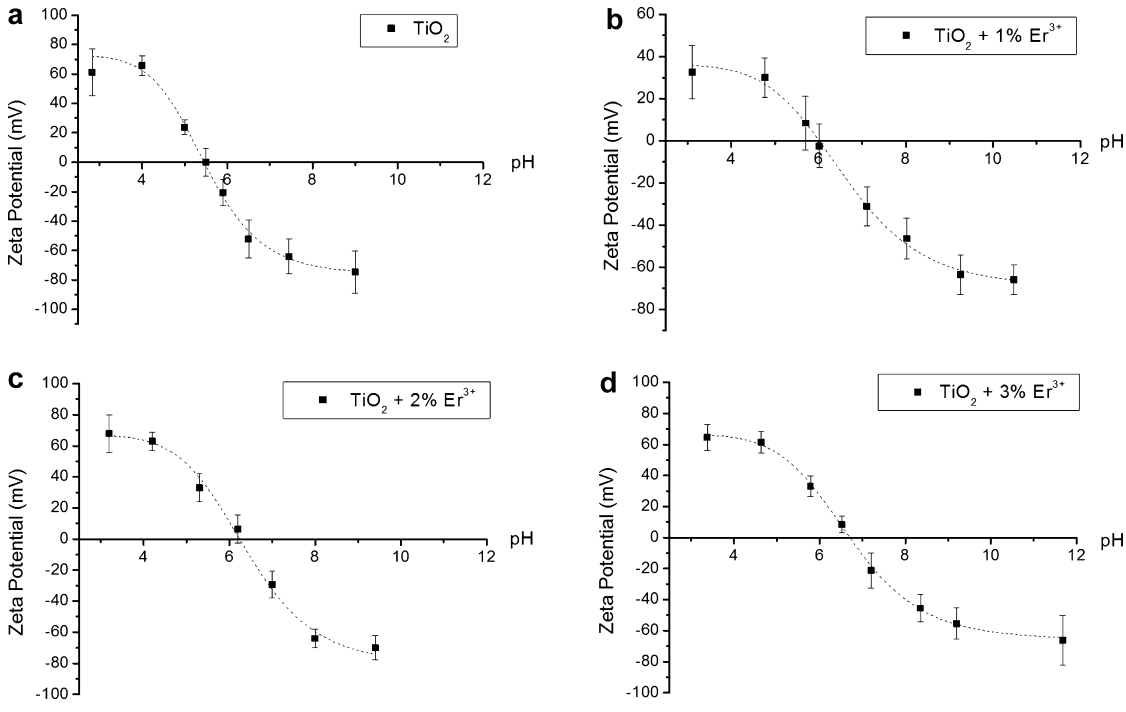

Figure 3. Evolution of zeta potential with pH for the TiO_2 (a) and TiO_2 + 1 (b), 2 (c), and 3 (d) mol % of Er^{3+} sols.

dx.doi.org/10.1021/jp304044w | J. Phys. Chem. B 2013, 117, 1556−1562

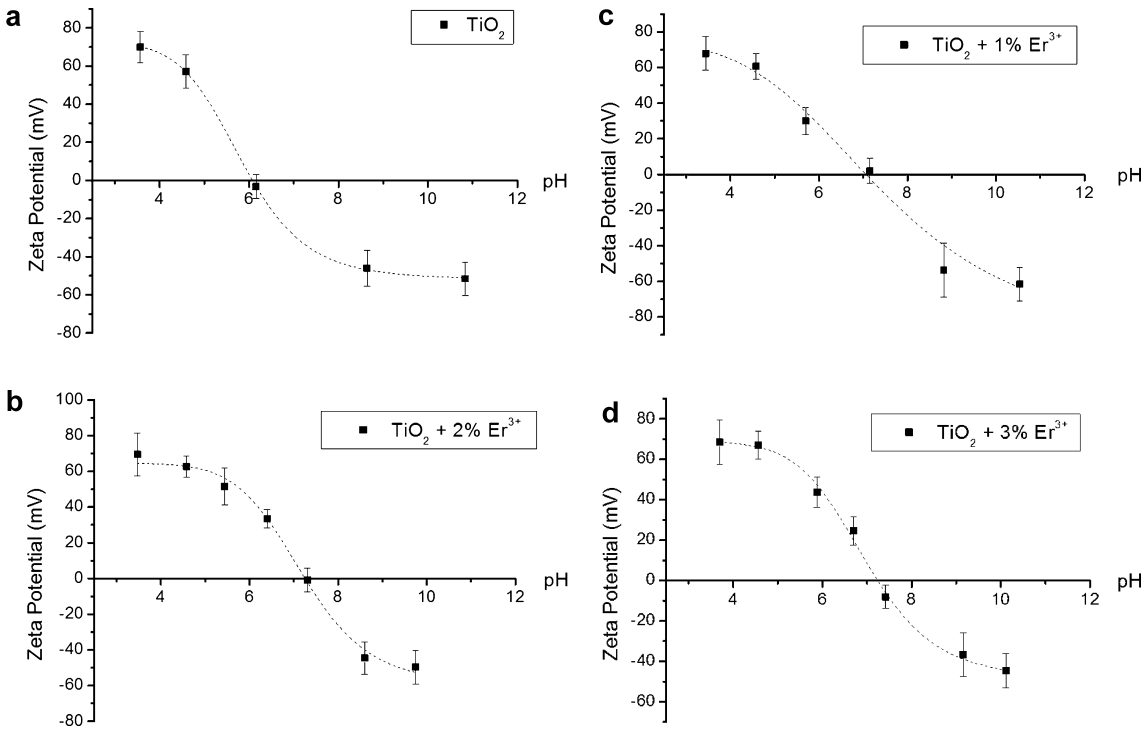

Figure 6. Evolution of zeta potential with pH for the TiO_2 (a) and TiO_2 + 1 (b), 2 (c), and 3 (d) mol % of Er^{3+} sols diluted in ethanol.

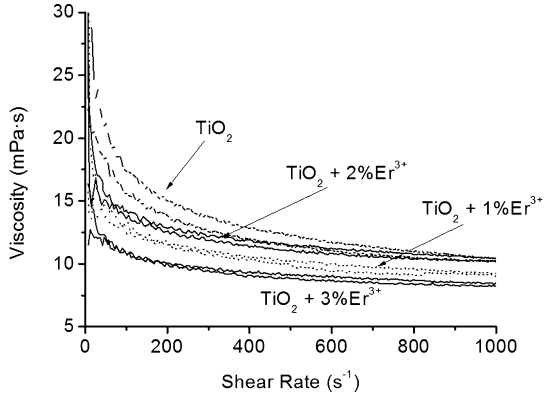

Figure 7. Viscosity curves of the peptized TiO_2 and TiO_2/Er^{3+} sols diluted in ethanol.

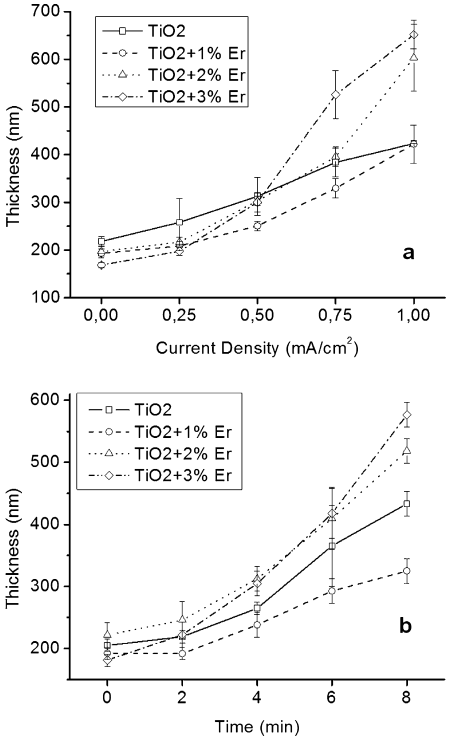

Figure 8. Evolution of the thin film thickness with the current density (a) and deposition time (b).

After this point, the DLS technique is needed to know the particle size which is in the range of nanometers ($D_{v,0.5}$ ~ 22 nm); moreover, the BS and T increase until an asymptotic value is reached due to the formation of the nanoparticles.

Figure 2 shows the viscosity curves of TiO_2 and TiO_2/Er^{3+} sols. All of them show a nearly Newtonian behavior, although an apparent increase of viscosity with the shear rate occurs in the TiO_2 and TiO_2 doped with 1 and 2 mol % of Er^{3+}; however, this is just related to the extremely low viscosity of those sols (3−5 mPa·s) that is within the detection limit of the rheometer. The TiO_2 sol with 3 mol % of Er^{3+} presents a higher viscosity that can be related to a higher amount of organic molecules (CH_3COOH, ^{i}PrOH) in the medium, which can react giving polymerization reactions and/or to the higher concentration of Er ions.

Zeta potential measurements were performed in 10^{-2} M KCl with a dilution of the sols of about 100 times. Figure 3 shows that the isoelectric point (IEP) for titania sol occurs at pH 5.5 which is in the range of the values found for anatase in the literature.[22,23] When Er^{3+} is present in the sol, the IEP shifts up to higher pHs, occurring at pH values of 5.9, 6.4, and 6.7 for sols with 1, 2, and 3 mol % of Er^{3+}. It indicates that erbium(III) is adsorbed onto the surface of TiO_2. In addition, the sols have a pH of ~1 and zeta potential values are positive at low pH's, thus meaning that the deposition of the nanoparticles would occur on the negative electrode.

dx.doi.org/10.1021/jp304044w | J. Phys. Chem. B 2013, 117, 1556−1562

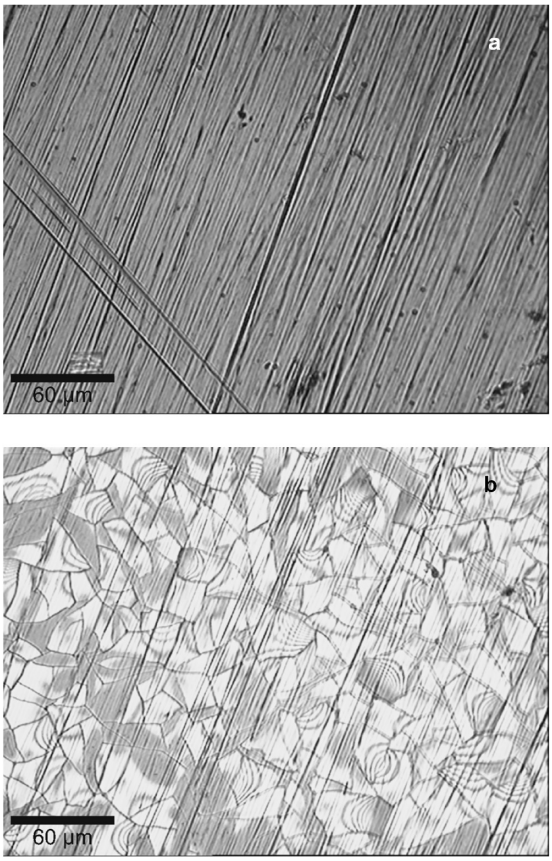

Figure 9. Optical microscope images of the transparent (a) and opal (b) thin films.

Xerogel Characterization. The xerogels were obtained drying the sols at room temperature and humidity. In all cases, the anatase phase as a major phase was confirmed by XRD, although some traces of brookite were also observed (Figure 4). Wide and poor defined peaks were obtained as expected for nanoparticulate xerogels. The crystal size calculated using eq 1 is shown in Table 1. In the case of the doped xerogels, the crystal size is quite similar and smaller than for the undoped one. Comparing these results with those obtained from DLS measurements, it is possible to conclude that the nanoparticles are formed by a few units of agglomerated crystals.

HRTEM images of the xerogel of TiO_2+2 mol % of Er^{3+} are shown in Figure 5, and the crystal size (D_{TEM}) observed (Table 1) is similar to that calculated by eq 1. The fast Fourier transformation (FFT) diagrams, shown as insets in each micrograph, provide direct evidence of the microstructure of the materials and confirm that the samples are polycrystalline. EDAX microanalysis proves the presence of erbium(III) in the appropriate amount (nominal composition), within the experimental error.

Thin Film Preparation and Characterization. Before starting the EPD experiments, a preliminary study of the withdrawal rate was performed ranging from 0.5 to 50 mm·s^{-1}. It was possible to observe that the homogeneity of the film was better at lower rates, and thus, a withdrawal rate of 0.5 mm·s^{-1} was used for further experiments.

Initially, EPD tests were done for the sols without any additive. Two different experiments were performed: (1) varying the current density (from 0.25 to 1 mA·cm^{-2}) at constant time (2 min) and (2) changing the deposition time (from 2 to 15 min) at a constant current density of 0.25 mA·cm^{-2}. In all cases, the homogeneity of the films increases when the erbium(III) amount increases, which could be related to the viscosity of the sols (higher viscosity, higher homogeneity); since this is a diluted colloidal sol, a higher viscosity helps to maintain the structure after dipping. Moreover, water plays an important role because its evaporation is more difficult than that of other solvents and hydrolysis takes place during the EPD experiments, which can contribute to decrease the homogeneity of the film due to the bubble formation. The thickness of the film did not change with the current density or the deposition time, as demonstrated by ellipsometry results. This fact could be explained by the presence of bubbles formed due to water hydrolysis which causes a detrimental effect in the thin film; in addition, due to the high value of the surface tension (~72 mN·m^{-2} at 25 °C),[24,25] water could separate the EPD deposited thin film from the substrate, obtaining a lower thickness associated only with the dipping process.

With the aim to improve these results, ethanol was added to the sol. A study was developed to obtain a film with the highest homogeneity. In this case, the best result was observed for ~55 wt % of ethanol. This new system presents a lower surface tension (~27 mN·m^{-2} at 25 °C)[25] and a faster evaporation, leading to increased homogeneity in comparison with the as-prepared sols. The addition of ethanol has some effect on the zeta potential and viscosity curves (Figures 6 and 7). In the first case, the isoelectric point (IEP) shifted up to higher pH's with regard to the initial sols, and in the case of the doped EtOH/H_2O systems, the IEP is the same in all cases. That suggests that new positive ions (i.e., $CH_3CH_2OH_2^+$) are adsorbed onto the TiO_2 surface. At lower pH's (EPD conditions), the zeta potential is positive and higher than the initial sols so that the mobility of the particles is expected to increase. Regarding the rheological behavior, the viscosity curves are quite similar (~9−12 mPa·s) and present a nearly Newtonian behavior. In the case of the TiO_2 and TiO_2 with 1 and 2 mol % of Er^{3+} EtOH/H_2O systems, the viscosity is higher compared to the initial sols; however, in the case of those doped with 3 mol % of Er^{3+}, the viscosity of the new system is lower. This can be related to the dilution effect produced when the ethanol is added and/or a possible polymerization reaction between the organic compounds present in the medium which would be catalyzed by the acid conditions.

The EPD experiments of the ethanol containing sols were performed under two different conditions: the first one is working at a constant time of 2 min, varying the current density from 0.25 to 1 mA·cm^{-2} and at a constant current density of 0.25 mA·cm^{-2} with different deposition times ranging from 2 to 15 min. Bubbles from water hydrolysis were not observed thanks to the addition of ethanol. Figure 8 shows the evolution of the thickness under the different conditions. In all cases, a clear difference can be observed between the dipping (time or current density = 0) and the EPD samples. Moreover, an increase of the thickness is well observed in all samples when either the current density or the deposition time increases, although for lower current densities and deposition times the thin film thickness is quite similar to that of dipping. It is also possible to see that the growth of the thickness of the thin film is faster (the slope is higher) when the erbium(III) amount increases, but for the TiO_2 system, the behavior is intermediate. In addition, the refractive index was obtained in each case from the ellipsometry measurements and is 1.95 ± 0.05 at 570 nm.

dx.doi.org/10.1021/jp304044w | J. Phys. Chem. B 2013, 117, 1556−1562

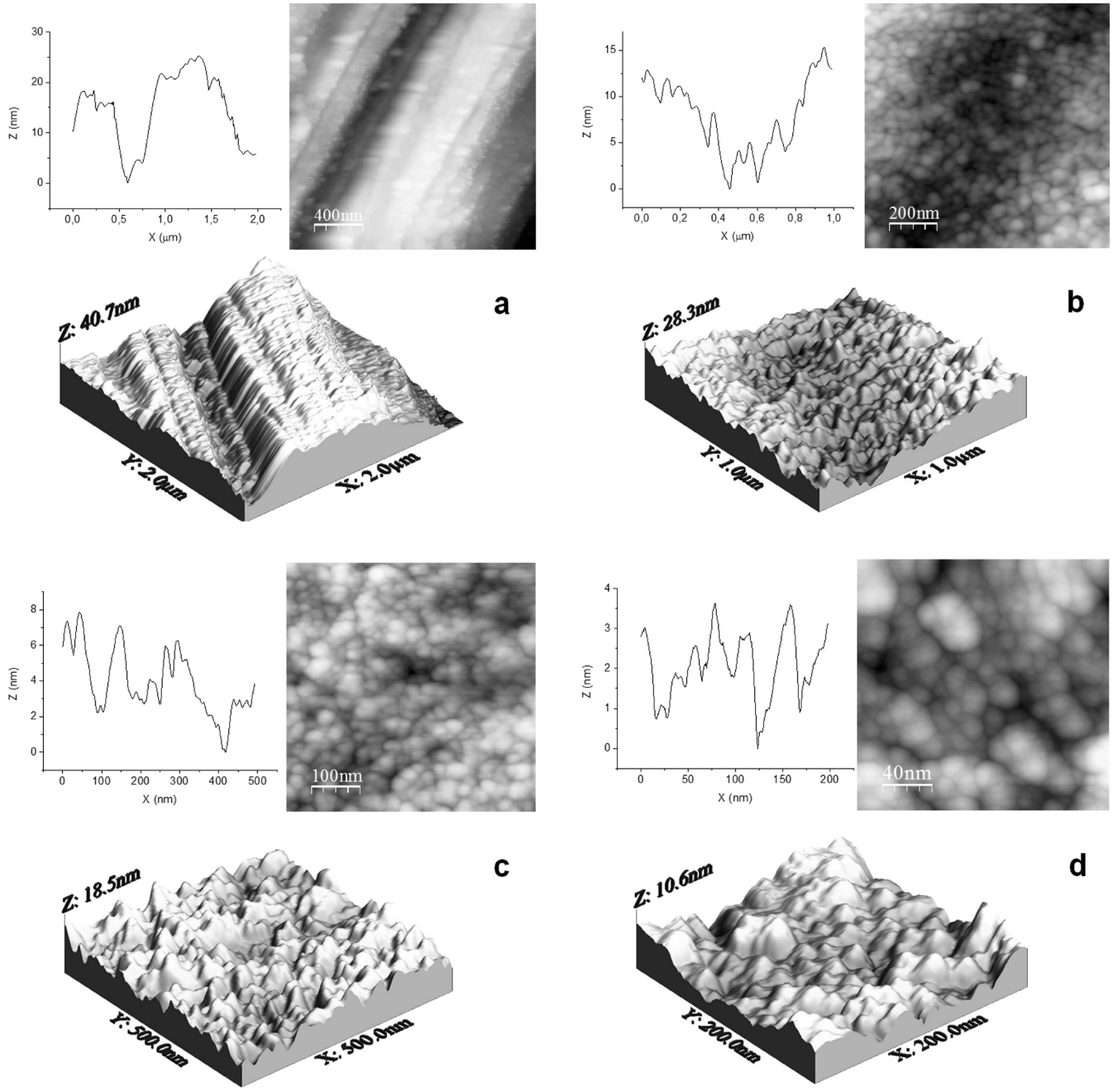

Figure 10. AFM images (topography channel) and roughness profile of the substrate (a) and TiO_2/Er^{3+} (1 mol %) thin film (b, c, and d).

This value increases as a function of the annealing temperature, in good agreement with observations reported by other authors.[26] At deposition times higher than 8 min, the thin films do not present uniform coloration (which indicates that they are not transparent) and they turn opal; thus, curve fitting obtained from the ellipsometric measurements becomes impossible. Probably, the deposited amount is higher and the deposition conditions change, not allowing the deposition of a uniform and transparent layer anymore. The image from optical microscopy in Figure 9a shows that for the transparent films it is possible to observe the defects of the steel substrate, whereas the image in Figure 9b shows that for the opal films there are cracks at the film surface.

Finally, the microstructure was observed by AFM (Figure 10). A general view of the topography of the substrate was recorded, showing that there are at least two different origins of roughness: big walls of 25−30 nm and smaller ones of 5 nm. Figure 10b and c shows the topography of the thin films at different scales. It is possible to observe the deposited nanoparticles whose size is in the range measured by DLS; it means that the addition of the ethanol does not provoke any agglomeration effect. In addition, two different roughnesses are observed as in the case of the substrate, which indicates that the surface of the substrate is covered homogeneously but the big walls are not totally blocked.

■ CONCLUSIONS

TiO_2 and TiO_2/Er^{3+} nanoparticulate sols were obtained by the colloidal sol−gel route. It was observed that the peptization time increases with the erbium(III) amount. In addition, the

dx.doi.org/10.1021/jp304044w | J. Phys. Chem. B 2013, 117, 1556−1562

zeta potential shifts up to higher pH's, which indicates that the Er^{3+} ions are adsorbed onto the surface of the titania nanoparticles.

The anatase phase was obtained in all cases as a major phase, and the crystal size was smaller than that observed by DLS measurements, indicating that few units of crystals are forming one nanoparticle.

EPD experiments show that the formation of the thin films using the aqueous sol is more difficult due to the deleterious effect of water hydrolysis and the high value of the surface tension of the water. When the sols are diluted in ethanol, the water hydrolysis was not observed and an increase of the thickness of the film with the current density or the deposition time occurs.

AUTHOR INFORMATION

Corresponding Author

*E-mail: rmoreno@icv.csic.es.

Notes

The authors declare no competing financial interest.

ACKNOWLEDGMENTS

This study has been supported by the Spanish Ministry of Economy and Competitiveness (MAT2009-14369-C02). M.B. thanks CSIC for the concession of a grant (JAE-Pre 083).

REFERENCES

(1) García, P.; Ferrari, B.; Moreno, R.; Sánchez-Herencia, A. J.; Colomer, M. T. *J. Eur. Ceram. Soc.* **2007**, *27*, 4241−4244.
(2) Besra, L.; Uchikoshi, T.; Suzuki, T. S.; Sakka, Y. *J. Eur. Ceram. Soc.* **2009**, *29*, 1837−1845.
(3) Kreethawate, L.; Larpkiattaworn, S.; Jiemsirilers, S.; Besra, L.; Uchikoshi, T. *Surf. Coat. Technol.* **2010**, *205*, 1922−1928.
(4) Moreno, R.; Ferrari, B. *Am. Ceram. Soc. Bull.* **2000**, *79*, 44−48.
(5) Kawakita, M.; Uchikoshi, T.; Kawakita, J.; Sakka, Y. *J. Am. Ceram. Soc.* **2009**, *92*, 984−989.
(6) Mazor, H.; Golodnitskya, D.; Burstein, L.; Gladkich, A.; Peled, E. *J. Power Sources* **2012**, *198*, 264−272.
(7) Lebrette, S.; Pagnoux, C.; Abélard, P. *J. Eur. Ceram. Soc.* **2006**, *26*, 2727−2734.
(8) Chen, H.-W.; Liao, Y.-T.; Chen, J.-G.; Wu, K. C.-W.; Ho, K.-C. *J. Mater. Chem.* **2011**, *21*, 17511−17518.
(9) Santillán, M. J.; Quaranta, N. E.; Boccaccini, A. R. *Surf. Coat. Technol.* **2010**, *205*, 2562−2571.
(10) Corni, I.; Ryan, M. P.; Boccaccini, A. R. *J. Eur. Ceram. Soc.* **2008**, *28*, 1353−1367.
(11) Fujishima, A.; Zhang, X.; Tryk, D. A. *Surf. Sci. Rep.* **2008**, *63*, 515−582.
(12) Chen, X.; Mao, S. S. *Chem. Rev.* **2007**, *107*, 2891−2959.
(13) Bavykin, D. V.; Lapkin, A. A.; Plucinski, P. K.; Friedrich, J. M.; Walsh, F. C. *J. Phys. Chem. B* **2005**, *109*, 19422−19427.
(14) Mignotte, C. *Appl. Surf. Sci.* **2004**, *226*, 355−370.
(15) Jeon, S.; Braun, P. V. *Chem. Mater.* **2003**, *15*, 1256−1263.
(16) Komuro, S.; Katsumata, T.; Kokai, H.; Morikawa, T. *Appl. Phys. Lett.* **2002**, *81*, 4733−4735.
(17) Patterson, A. L. *Phys. Rev.* **1939**, *56*, 978−982.
(18) Herzinger, C.; Johs, B.; McGahan, W. A.; Woollam, J. A.; Paulson, W. *Appl. Phys.* **1998**, *83*, 3323−3336.
(19) Horcas, I.; Fernández, R.; Gómez-Rodríguez, J. M.; Colchero, J.; Gómez-Herrero, J.; Baro, A. M. *Rev. Sci. Instrum.* **2007**, *78*, 013705.
(20) Colomer, M. T.; Guzmán, J.; Moreno, R. *Chem. Mater.* **2008**, *20*, 4161−4165.
(21) Colomer, M. T.; Guzmán, J.; Moreno, R. *J. Am. Ceram. Soc.* **2010**, *93*, 59−64.
(22) Kosmulski, M. *J. Colloid Interface Sci.* **2011**, *353*, 1−15.
(23) Fazio, S.; Guzmán, J.; Colomer, M. T.; Salomoni, A.; Moreno, R. *J. Eur. Ceram. Soc.* **2008**, *81*, 2171−2176.
(24) Vazquez, G.; Alvarez, E.; Navaza, J. M. *J. Chem. Eng. Data* **1995**, *40*, 611−614.
(25) Landolt-Börnstein, *Numerical Data and Functional Relationships in Science and Technology, New Series, IV/16, Surface Tension*; Springer-Verlag: Heidelberg, Germany, 1997.
(26) Bahtat, A.; Bouazaoui, M.; Bahtat, M.; Garapon, C.; Jacquier, B.; Mugnier, J. *J. Non-Cryst. Solids* **1996**, *202*, 16−22.